Cell Biol Toxicol (2019) 35:345–360
https://doi.org/10.1007/s10565-019-09460-0

ORIGINAL ARTICLE

Protein carbonylation in human bronchial epithelial cells exposed to cigarette smoke extract

Graziano Colombo · Maria Lisa Garavaglia · Emanuela Astori · Daniela Giustarini · Ranieri Rossi · Aldo Milzani · Isabella Dalle-Donne

Received: 14 September 2018 / Accepted: 2 January 2019 / Published online: 16 January 2019

Abstract Cigarette smoke is a well-established exogenous risk factor containing toxic reactive molecules able to induce oxidative stress, which in turn contributes to smoking-related diseases, including cardiovascular, pulmonary, and oral cavity diseases. We investigated the effects of cigarette smoke extract on human bronchial epithelial cells. Cells were exposed to various concentrations (2.5–5–10–20%) of cigarette smoke extract for 1, 3, and 24 h. Carbonylation was assessed by 2,4-dinitrophenylhydrazine using both immunocytochemical and Western immunoblotting assays. Cigarette smoke induced increasing protein carbonylation in a concentration-dependent manner. The main carbonylated proteins were identified by means of two-dimensional electrophoresis coupled to MALDI-TOF mass spectrometry analysis and database search (redox proteomics). We demonstrated that exposure of bronchial cells to cigarette smoke extract induces carbonylation of a large number of proteins distributed throughout the cell. Proteins undergoing carbonylation are involved in primary metabolic processes, such as protein and lipid metabolism and metabolite and energy production as well as in fundamental cellular processes, such as cell cycle and chromosome segregation, thus confirming that reactive carbonyl species contained in cigarette smoke markedly alter cell homeostasis and functions.

Keywords Cigarette smoke extract (CSE) · 2D-electrophoresis · Human bronchial epithelial cells (16-HBE cells) · Matrix-assisted laser desorption/ionization (MALDI) · Protein carbonylation

G. Colombo (✉) · M. L. Garavaglia · E. Astori · A. Milzani · I. Dalle-Donne
Department of Biosciences, Università degli Studi di Milano, via Celoria 26, 20133 Milan, Italy
e-mail: graziano.colombo@unimi.it

D. Giustarini · R. Rossi
Department of Biotechnology, Chemistry and Pharmacy, University of Siena, 53100 Siena, Italy

Introduction

Accumulated epidemiological evidences support the strong correlation between smoking and diseases such as lung respiratory (Wong et al. 2016; Morse and Rosas 2014) and cardiovascular diseases (Morris et al. 2015), cancer (Alberg et al. 2013), and oral cavity disorders (Dietrich et al. 2004). In particular, cigarette smoking is related to pulmonary pathologies, such as chronic obstructive pulmonary disease (COPD) and lung cancer, which represent the leading cause of mortality and morbidity in the worldwide population (Alberg et al. 2013). In addition, well-established positive anamnestic correlations were demonstrated also between cigarette smoke and a number of autoimmune diseases, including systemic lupus erythematosus (Mak and Tay 2014), Behcet's disease (Perricone et al. 2016), rheumatoid arthritis (Afridi et al. 2014; Talbot et al. 2018), ankylosing spondylitis, psoriasis (Armstrong et al. 2014),

systemic and multiple sclerosis (Costenbader and Karlson 2006), inflammatory bowel disease (Yadav et al. 2017), autoimmune liver, and thyroid disease (Bose 2015). Despite political and social approaches to limit smoking, cigarette smoke (CS) habit still remains a widespread clinical issue.

CS consists of a complex mixture of chemicals, several hundred of which are known to be toxic and detrimental to the physiology of many organs. Many studies elucidated mechanisms involved in CS-induced inflammation (Chang et al. 2011; Xueshibojie et al. 2016), DNA damage (Jang et al. 2014), autophagy (Dong et al. 2015; Bodas et al. 2016), and the subsequent cell fates (Bucchieri et al. 2015), including cell death (Tesfaigzi 2006), cellular senescence (Bodas et al. 2016; Liu et al. 2016), and transformation (Bersaas et al. 2016). Although CS has been implicated in multiple pathologies, the cellular and molecular mechanisms of CS-induced pathological effects remain inadequately understood. This can be attributed, in part, to the difficulty in deciphering which of the individual CS components are the major causative agents.

The small airways are an important site of CS-induced pathology exacerbation (Thorley and Tetley 2007). The structural alteration of small airways is believed to have the greatest influence on airflow limitation (Hogg et al. 2013), and precedes emphysematous changes observed in COPD, with chronic airway inflammation as a key feature (McDonough et al. 2011). The epithelium in peripheral bronchioles of smokers shows an increased number of inflammatory cells (Mortaz et al. 2011), fibrosis (Adesina et al. 1991), and metaplasia of goblet cells (Saetta et al. 2000) that leads to overproduction of mucus, providing a prime site for bacterial colonization (Sethi et al. 2000; Aiassa et al. 2011), further aggravating the inflammatory response. The expression of inflammatory mediators is chiefly induced by redox-sensitive signalling pathways activated after exposure to CS, and it promotes chronic immune cell recruitment. The burning cigarette produces thousands of reactive oxygen and nitrogen species (ROS and RNS), which are not withdrawn by cigarette filters (Huang et al. 2005). ROS are extremely reactive short-living molecules affecting primarily the epithelial cells lining the upper airways, by inducing protein oxidation, peroxidation of lipids and DNA damage, and by activating oxidative stress-sensitive cellular pathways (Rahman 2005). Therefore, oxidative stress is an important mechanism implicated in the pathogenesis of COPD and it amplifies inflammation induced by CS (Brusselle et al. 2011).

A prevailing oxidative modification of proteins is carbonylation, a non-enzymatic process yielding to the (mostly irreversible) formation of several carbonyl (CO) groups in the form of aldehyde or ketone. Carbonyl groups may be introduced within the protein structure at different sites and following numerous mechanisms: (1) oxidative cleavage of the protein backbone by either the α-amidation pathway or oxidation of glutamyl side chains leading to the formation of polypeptide fragments in which the *N*-terminal amino acid is blocked by an α-ketoacyl derivative; (2) direct oxidation of proline, arginine, lysine, and threonine side chains producing, respectively, 2-pyrrolidone (Pro) or glutamic semialdehyde (Pro and Arg), aminoadipic semialdehyde, and 2-amino-3-ketobutirric acid; (3) addition of reactive carbonyl species generated during lipid peroxidation (e.g., HNE, acrolein, and malondialdehyde) to the nucleophilic side chain of cysteine, histidine, or lysine, leading to the formation of advanced lipoxidation end products (ALEs); and (4) addition to proteins of reactive carbonyl derivatives (e.g., 3-deoxyglucosone, dideoxysones, methylglyoxal, and glyoxal) generated by oxidation of sugars, ascorbate, polyunsaturated fatty acids, or Schiff base species resulting from the reaction of lysine residues with reducing sugars, or by direct oxidation of the Amadori adducts resulting from the latter species, giving rise to advanced glycation end products (AGEs) (Berlett and Stadtman 1997; Dalle-Donne et al. 2003; Dalle-Donne et al. 2006; Bachi et al. 2013). Protein carbonylation is believed to trigger functional inactivation of crucial cell proteins, to induce protein aggregation and proteasome inhibition by glycoxidation and lipid peroxidation products (Sultana et al. 2013; Pizzimenti et al. 2013). Protein aggregates are a direct consequence of their structural damage, and they can in turn modify the cellular metabolism, thus influencing cell functionality (Martínez et al. 2010; Castro et al. 2012). Therefore, protein carbonylation is a well-acknowledged biomarker of oxidative stress related diseases (Feng et al. 2008; Dalle-Donne et al. 2006).

Limited information is available on the oxidative effects of CS in human bronchial epithelial cells. Exposure to cigarette smoke extract (CSE) increases ROS production, expression of nuclear factor E2-related factor 2 (Nrf2), and expression of several antioxidant enzymes such as haeme oxygenase-1,

glutathione peroxidases 2 and 3, glutathione disulphide reductase, and glutamate-cysteine-ligase as well as to decrease intracellular GSH concentration (Bazzini et al. 2013; Pace et al. 2013; Bondì et al. 2014; Wu et al. 2016). In this work, we aimed to evaluate the oxidative effects of CSE on the proteome of human bronchial epithelial cells by means of redox proteomics.

Materials and methods

Materials

Iodoacetamide, 2,4-dinitrophenylhydrazine (DNPH) and ProteoSilver™ Plus Kit were purchased from Sigma-Aldrich (Milan, Italy). Anti-dinitrophenyl-KLH (anti-DNP) antibodies, rabbit IgG fraction and goat anti-rabbit IgG, and horseradish peroxidase conjugate were purchased from Molecular Probes (Eugene, OR, USA). Urea, thiourea, 3-((3-cholamidopropyl)-dimethylammonio)-1-propanesulfonate (CHAPS), Immobiline DryStrips 3–10, IPG Buffer 3–10, streptavidin-HRP, and ECL Plus Western blotting detection reagents were obtained from GE Healthcare (Milan, Italy). ProteaseMAX™ surfactant and modified sequencing grade trypsin were purchased from Promega (Madison, WI, USA). All other reagents were of analytical grade (Sigma-Aldrich, Milan, Italy).

Cell line and solutions for cell maintenance

16-HBE 14o- (16-HBE) cells, an immortalized normal human bronchial epithelial cell line, were grown in collagen/fibronectin-coated plates with Eagle's Minimum Essential Medium (EMEM) supplemented with 10% fetal bovine serum (FBS), 2 mM L-glutamine, 0.1 mM non-essential amino acids, 100 U/ml penicillin, and 100 μg/ml streptomycin (Sigma, Italy). Cell cultures were maintained at 37 °C with 5% CO_2 and passaged every 3–4 days. For experiments, 16-HBE cells were cultured in the presence or absence of different concentrations of CSE for 1, 3, or 24 h.

Preparation of CSE solutions

CSE was prepared immediately before use as described by colleagues with some modifications (Su et al. 2004). After the removal of the filter, three cigarettes (Marlboro, Philip Morris, Inc., Richmond, VA, containing 10 mg of tar and 0.8 mg of nicotine) were bubbled into 30 ml of phosphate-buffered saline (PBS, 136.9 mM NaCl, 2.7 mM KCl, 3.2 mM Na_2HPO_4, 1.5 mM KH_2PO_4). The CSE solution was filtered through a syringe with a 0.45-μm pore-sized filter to remove bacteria and particulate. The concentration of CSE was calculated spectrophotometrically by measuring the optical density at a wavelength of 320 nm. This solution was considered to be 100% CSE and was diluted to the concentrations of 2.5, 5, and 10%, keeping the PBS/EMEM proportion fixed to 1:10. Controls were made by adding PBS to the medium (1:10). The CSE concentrations used correspond approximately to exposures associated with smoking slightly less than 0.5 pack of cigarettes (there are 20 cigarettes in a pack) a day (2.5%) to slightly less than 2 packs a day (10%) (Su et al. 2004).

MTT assay

Cells in the logarithmic growth phase (80% confluence) were seeded on flat bottom 24-well culture plates with a cell density of 4000 cells/well (2000 cells/cm^2), with 1 ml of complete growth medium in each well. After 24 h in culture, cells were evenly attached to the well bottom and were then exposed to different concentrations (2.5%, 5%, 10%, and 20%) of CSE. After incubation, the medium was substituted with 3-[4,5-dimethylthiazol-2-yl]-2,5-diphenyltetrazoliumbromide (MTT) at the concentration of 0.5 mg/ml in complete growth medium. After a 3-h incubation at 37 °C, the MTT solution was removed and cells were lysed in 90% DMSO/10% Sorensen's glycine buffer (0.1 M glycin, 0.1 M NaCl, pH 10.5). Absorbance (A) was measured at 570 nm with an Ultrospec 300 spectrophotometer (Pharmacia Biotech). Values were subtracted of the absorbance value readings at 630 nm. Four independent complete series (each comprising control, 2.5%, 5%, 10%, 20% CSE) were assayed. In each series, every condition was measured in triplicate.

Cell counting

Cells in the logarithmic growth phase (80% confluence) were seeded on flat bottom 24-well culture plates with a cell density of 4000 cells/well (2000 cells/cm^2), with 1 ml of complete growth medium in each well. After 24 h in culture, cells were evenly attached to the well bottom. The cell medium was changed every 24 h. CSE

at various concentrations (as defined in the text) was added to the complete medium, and the cells were cultured for 9 days. Cell concentration was recorded from four wells every 24 h using a haemocytometer. For each well, cells were harvested and counted in four squares of the haemocytometer. Cell growth rate was calculated every 24 h as the slope of the connecting line between two successive records.

Cell migration assay

Cells in the logarithmic growth phase (80% confluence) were seeded on 12-mm diameter round coverslips (10^5 cells/well). At cell confluence, the coverslips were settled upside down in a 24-well culture plate coated with collagen and fibronectin in the presence of complete medium and PBS (control) or 5, 10, and 20% CSE for 24 h. Cells were then fixed by the addition of 4% paraformaldehyde in PBS and stained with crystal violet in 2% ethanol for 15 min. Images were acquired with an inverted microscope (Axiovert 200, Zeiss, Oberkochen, Germany) equipped with a photometric CoolSNAP CCD camera (Roper Scientific, Trenton, NJ, USA), and the distance of cell migration was quantitatively evaluated using the ImageJ 1.40d software (National Institutes of Health, Bethesda, MD, USA).

Western blot analysis of carbonylated proteins

Cells were scraped in lysis buffer (50 mM Tris–HCl pH 7.4, 150 mM NaCl, 1% Triton X-100, 0.1% SDS, 0.5% Na-deoxycholate and proteases inhibitors (Sigma P8340)) and incubated 30 min in ice. Cell extracts were centrifuged 10,000*g* for 5 min, and supernatants were used for BCA protein assay. Carbonylated proteins were derivatized with DNPH (Colombo et al. 2016). Briefly, 200 μg (1 mg/ml) of whole protein cell lysates were mixed with 40 μl of 10 mM DNPH in 2 N HCl and incubated for 60 min in the dark. Samples were then mixed with 240 μl of 20% trichloroacetic acid (TCA) and incubated for 10 min in ice. After centrifugation at 20,000*g* for 15 min at 4 °C, protein pellets were washed three times with 1:1 ethanol/ethylacetate to remove free DNPH. Air-dried protein pellets were resuspended in 2× reducing Laemmli sample buffer. Proteins were separated by SDS-PAGE on 12% (*w*/*v*) Tris–HCl polyacrylamide gels, transferred to PVDF membrane, and detected through Western immunoblotting with anti-DNP antibody (Colombo et al. 2012; Gornati et al. 2013). Immunoreactive protein bands were visualized by ECL detection.

2-D PAGE

Each sample containing 200 μg of proteins was precipitated using a chloroform/methanol protocol and resuspended in a solution containing 7 M urea, 2 M thiourea, and 4% CHAPS (Colombo et al. 2009). Solubilized samples were used to rehydrate immobilized pH gradient (IPG) strips just before isoelectrofocusing. For the first-dimension electrophoresis, samples were applied to IPG strips (11 cm, pH 3–10 linear gradient). Strips were rehydrated at 20 °C for 1 h without current and for 12 h at 30 V in a buffer containing 7 M urea, 2 M thiourea, 4% CHAPS, 1 mM dithiothreitol (DTT), and 1% IPG buffer 3–10. Strips were focused at 20 °C for a total of 70,000 V/h at a maximum of 8000 V using the Ettan IPGphor II system (GE Healthcare). The focused IPG strips were stored at − 80 °C until second-dimension electrophoresis was performed. For the second dimension, IPG strips were equilibrated at room temperature for 15 min in a solution containing 6 M urea, 2% SDS, 30% glycerol, 50 mM Tris–HCl (pH 8.8), and 10 mg/ml DTT and then re-equilibrated for 15 min in the same buffer containing 25 mg/ml iodoacetamide in place of DTT. The IPG strips were placed on top of a 12% polyacrylamide gel, and proteins were separated at 25 °C with a pre-run step at 20 mA/gel for 1 h and a run step at 30 W/gel for 3.5 h. After run, gels were fixed and stained with Sigma ProteoSilver Plus silver stain according to the manufacturer's specifications (Sigma-Aldrich).

In-gel trypsin digestion and protein identification by MALDI-TOF MS analysis

Protein spots were manually excised from silver-stained 2D gels with a razor blade, chopped into 1 mm^3 pieces, and collected into a LoBind tube (Eppendorf). Gel pieces were destained with Silver destaining solutions, washed with 100 μl of 50% (*v*/*v*) acetonitrile in 50 mM ammonium bicarbonate (pH 7.4), dehydrated in 100 μl of acetonitrile for 5 min, and completely dried in a SpeedVac (ThermoSavant) after solvent removal. Digestion was performed for 2 h a 37 °C with sequencing grade modified trypsin diluted in ProteaseMAX™ surfactant. Digested samples were centrifuged at 16,000*g* for 10 s, and the digestion reaction with extracted

peptides was transferred into a new tube. Trifluoroacetic acid was added to a final concentration of 0.5% to inactivate trypsin. Finally, samples were reduced to ~ 5 μl in SpeedVac. One-microliter aliquots of the trypsin-digested protein supernatant were used for MS analysis on an AutoFlex MALDI-TOF (Bruker) mass spectrometer. Peak list was obtained by peak de-isotoping. Spectra were accumulated for over a mass range of 750–4000 Da with a mean resolution of about 15,000. Alkylation of Cys by carbamidomethylation and oxidation of Met were considered as fixed and variable modifications, respectively. Two missed cleavages per peptide were allowed, and an initial mass tolerance of 50 ppm was used in all searches. Peptides with masses correspondent to those of trypsin and matrix were excluded from the peak list. Proteins were identified by searching against a comprehensive non-redundant protein database using MASCOT programs via the internet.

Immunodetection of intracellular carbonylated proteins

Cells, seeded on 12-mm diameter round coverslips (10^5 cells/well) and exposed to PBS, 5, 10, and 20% CSE for 24 h, were fixed and permeabilized by incubation with methanol (5 min at − 20 °C), washed thoroughly with TBS (50 mM Tris–Cl, 150 mM NaCl pH 7.5) and covered with 0.1% DNPH in 2 N HCl for 1 h at room temperature. After several washing steps with TBS, cells were blocked with 1% normal goat serum in TBS (30 min at room temperature) and incubated with an anti-DNP antibody (1:500) overnight at 4 °C. After washing steps with PBS, cells were incubated with secondary antibody (an anti-rabbit-TRITC conjugated diluted 1:200 in PBS + 0.5% BSA) and the coverslips mounted onto glass slides on a drop of aqueous-based mounting medium (Fluoromont, Sigma). Fixed cells were imaged with a ViCo confocal microscope (Nikon).

Results

CSE alters growth rate of 16-HBE cells

The growth curves of cultured 16-HBE cells were followed up to 120 h. By using trypan blue exclusion analysis (Fig. 1a) and MTT assay (Fig. 1b), we observed that, after exposure to 2.5–20% CSE, the growth rate was dose-dependently decreased. Control 16-HBE cells followed an exponential growth curve, whereas 2.5% and 5% CSE-treated cells showed a significant reduction in growth over time after exposure to CSE. Cells treated with 10% CSE showed a trend similar to 5% CSE treated cells for the first 96 h in culture, but they failed to growth for longer time. Growth curves obtained from trypan blue and MTT assays are qualitatively superimposable, and they confirm that exposure to 2.5% and 5%-CSE was compatible with cell viability for more than 96 h. Exposure of 16-HBE cells to 10% and 20% CSE caused a drastic lowering of the levels of cellular metabolic activity (Fig. 1b). Growth data from trypan blue exclusion analysis were fitted according to Gompertz equation. This analysis allowed us to estimate that control cells grew at a rate of 4363 cells/h compared to 5%-CSE treated cells growing at a rate of 1359 cells/h (Fig. 1c). A similar trend was also observed when MTT assay data were used to compare growth rates of control cells and 5% CSE-treated cells (Fig. 1d).

CSE reduces cell migration ability of 16-HBE cells

The migration ability of cultured 16-HBE cells, determined 24 h after exposure to CSE, was visualized with an inverted microscope after fixation and crystal violet staining (Fig. 2a). Control 16-HBE cells demonstrated a more efficient migration in comparison with CSE-treated cells. Control cells developed a thicker growth layer relative to CSE-treated cells, and their shape was more regular and orderly organized than that of CSE-treated cells. In particular, a well-organized and compact cellular growth layer was evident in control cells and cells exposed to 5% CSE, whereas a thinner cellular growth layer was observed in cells exposed to 10% CSE and a reduced and disorganized one was evident in cells exposed to 20% CSE. As a whole, the growth rate and migration ability of cultured 16-HBE cells were dose-dependently and significantly decreased following the treatment with CSE, as shown in the box plot of Fig. 2b.

CSE induces protein carbonylation in 16-HBE cells

Protein carbonylation represents an index of mostly irreversible oxidation, which can be assayed by immunochemical and Western blotting methods after reaction of carbonyl groups with DNPH and consequent formation of the DNP adducts. Immunocytochemical techniques were used to determine the formation of carbonylated molecules in 16-HBE cells exposed to 5–20% CSE for 3 (Fig. 3a, upper line) and 24 h (Fig. 3a,

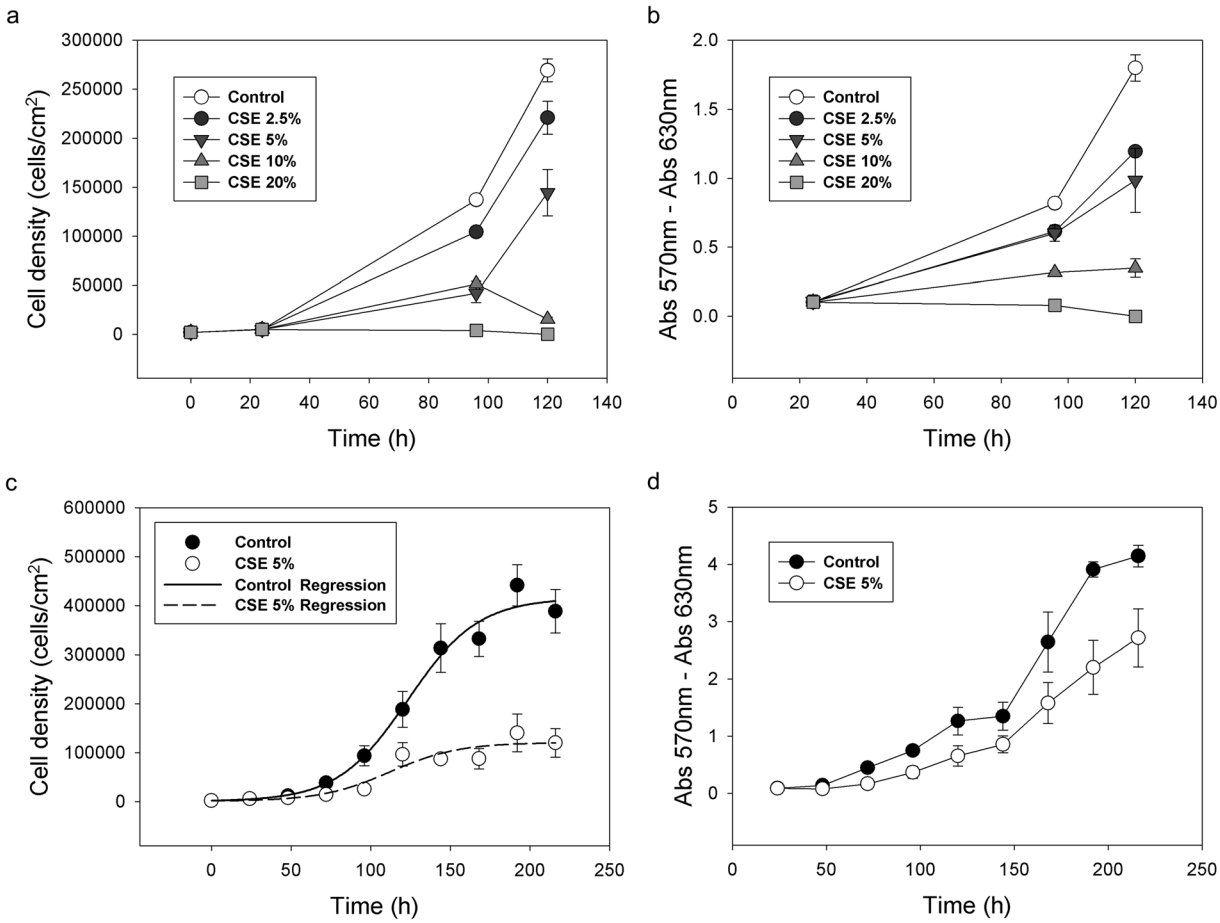

Fig. 1 Cell density and metabolic activity of 16-HBE cells exposed to CSE. **a** Graphic representation of growth rates (shown as cell density ± SEM) of control and CSE-treated cells up to 120 h measured by trypan blue exclusion assay with haemocytometer counting. **b** Graphic representation of cellular proliferation measured by MTT assay (shown as the difference between absorbance at 570 nm and 630 nm). Control and CSE-treated cells up to 120 h are represented. **c** A comparison of cell growth (shown as cell density) between control and 5% CSE-treated cells (up to 220 h of treatment) is shown. A regression curve for each condition is drawn according to Gompertz growth equation. **d** A comparison between proliferation (MTT assay shown as the difference between absorbance at 570 nm and 630 nm) of control and 5% CSE-treated cells (up to 220 h of treatment) is shown

middle line). The fixed cells were incubated with DNPH solution to derivatize carbonyl groups, then with anti-DNP antibody, and finally with an anti-rabbit TRITC-conjugated secondary antibody. The fluorescence signal increased with the increase in CSE concentration, and it was already evident after cell exposure to 5% CSE for 3 h (Fig. 3a, upper line). A similar result was observed after 24 h of cell exposure to CSE, though a fainter signal was observed compared to the same CSE concentration after 3 h exposure (Fig. 3a, middle line). As shown in the bottom line of Fig. 3a (representing a 4× magnification of the middle line), carbonylation is widespread throughout the cytoplasm and the nucleus and it is CSE concentration-dependent. In particular, the immunostaining indicates abundant and diffuse presence of carbonylation within the cells after exposure to 10% and 20% CSE.

We investigated protein carbonylation in whole-cell lysates by Western immunoblotting (Fig. 3b), confirming that protein carbonylation increased in a dose-dependent manner with the CSE concentration, at all times of exposure. In particular, a significant increase in protein carbonylation was observed in protein lysates from 16-HBE cells exposed to 2.5, 5%, and 10% CSE compared to control ones at all times of treatment (Fig. 3b). Interestingly, a marked decrease in protein carbonylation was observed after 24 h of cell exposure to all CSE concentrations compared to 1 h and 3 h exposure.

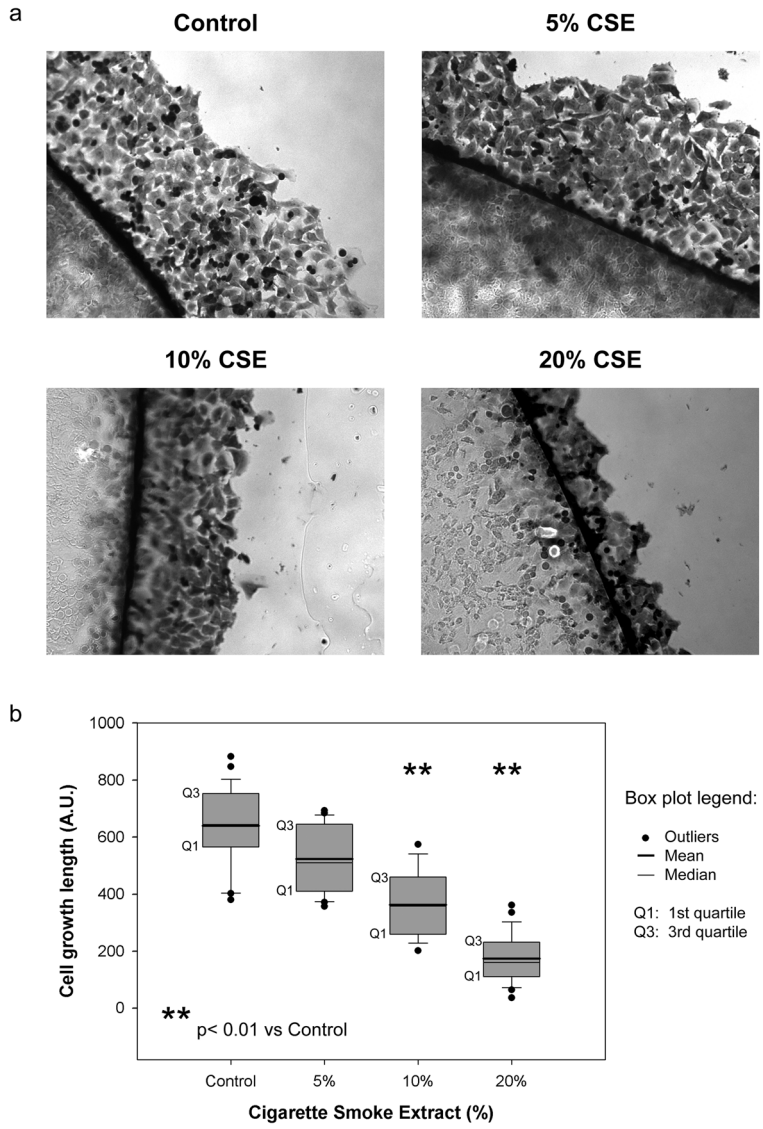

Fig. 2 Migration assay in 16-HBE cells exposed to CSE. **a** Cells were grown at confluence on a glass surface and then the coverslips were settled upside down in a 24-well culture plate coated with collagen and fibronectin in the presence of complete medium and PBS (control) or 5, 10, and 20% CSE for 24 h. Four pictures representing cell growth after exposure to different percentages of CSE are shown (control, top left; 5% CSE, top right; 10% CSE, bottom left; 20% CSE, bottom right). **b** Box-plot showing the distribution of the thickness of the layer of cellular growth after a 24 h exposure to CSE. The thickness was directly measured on pictures, and the result of at least 200 measurements for condition was represented. Percentiles were computed according to standard method and asterisks indicate a significant difference in comparison with control condition. $^{**}p < 0.01$ one-way ANOVA, post-hoc Tukey's test

With the aim of identifying possible molecular targets of CSE-induced carbonylation, protein extracts were separated by 2-D PAGE (Fig. 4a) and several carbonylated proteins were identified in 16-HBE cells exposed to 5% CSE for 3 h by means of redox proteomics (Colombo et al. 2012).

Comparing the 2-D pattern on the blot of carbonylated proteins from 5% CSE-treated cells (Fig. 4c) to the 2-D pattern on the MS-compatible silver-stained polyacrylamide gel of the same sample (Fig. 5) and using spot isoelectric point and molecular weight as references, we selected protein spots to be excised from the gel and to be identified by MALDI-TOF technology. Using a MALDI-TOF MS approach and an associated MASCOT database search, we identified 26 highly carbonylated proteins against all human proteins in the SwissProt database (Fig. 5 and Table 1).

Classification of carbonylated proteins

Using the PANTHER (Protein ANalysis THrough Evolutionary Relationships) Classification System (http://www.pantherdb.org), we gathered carbonylated proteins according to their involvement in biological processes (Fig. 6a) and their molecular functions (Fig. 6b). According to the first classification, 33% of carbonylated proteins is involved in metabolic processes, mainly in primary metabolism, generation of energy, biosynthesis, and

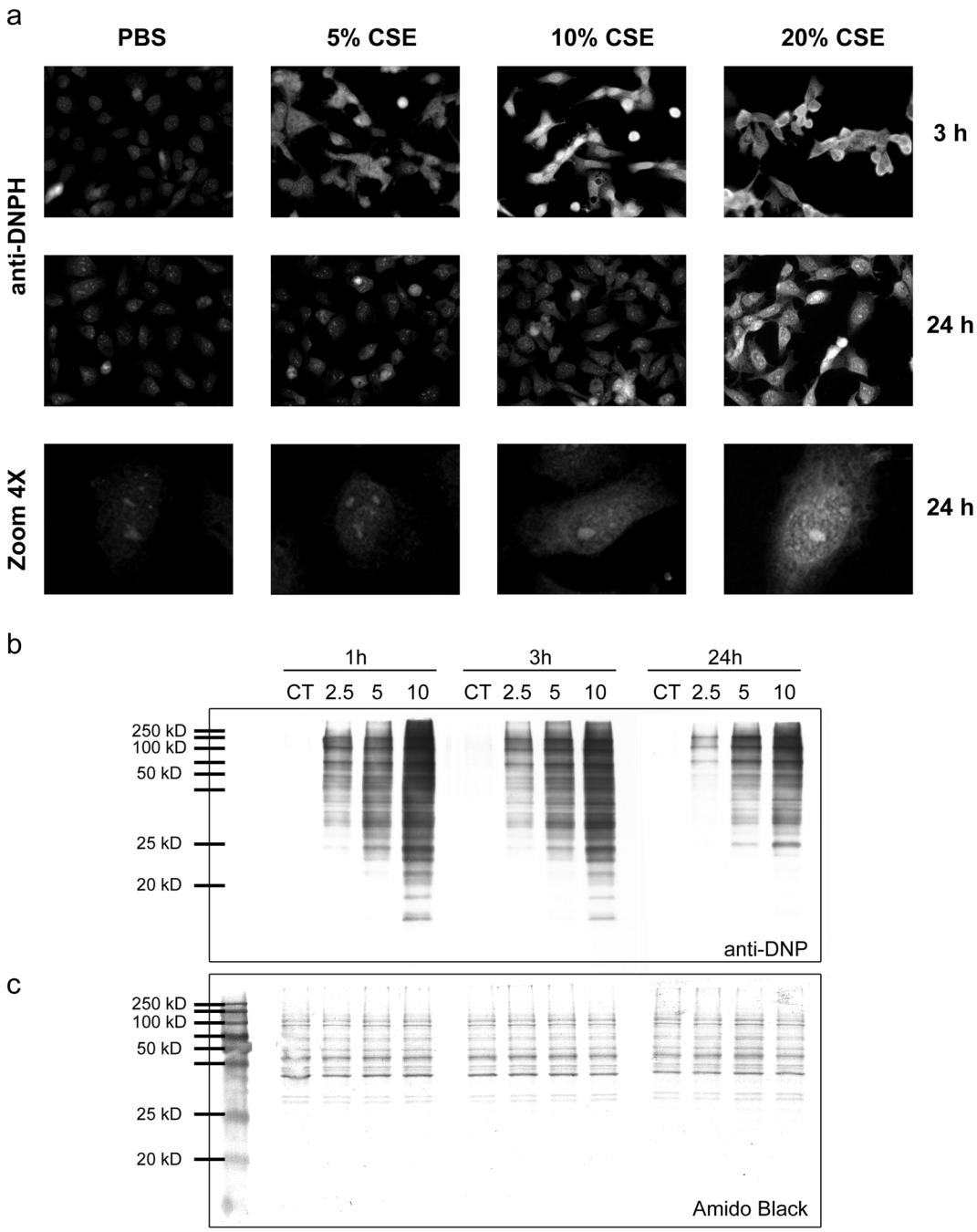

Fig. 3 Carbonylation in 16-HBE cells exposed to CSE. **a** Immunofluorescence showing global carbonylation after 3 h (upper line) and 24 h (middle line) of exposure to CSE. The bottom line shows a 4× magnification of the images of the middle line. **b** Protein carbonylation in whole-cell lysates from 16-HBE cells exposed to 0, 2.5, 5, and 10% CSE for 1, 3, and 24 h. A representative Western blot of the protein carbonylation pattern is shown. No immunostaining was observed in parallel experiments in which either the protein samples were treated with $NaBH_4$ or the primary antibody to DNP was omitted (not shown). **c** The corresponding Amido black-stained PVDF membrane is shown to highlight equal protein loading in each lane

catabolic pathways whereas 28% of carbonylated proteins takes part in cellular processes, mainly cell cycle, chromosome segregation, cell communication, and movement. The involvement of carbonylated proteins in

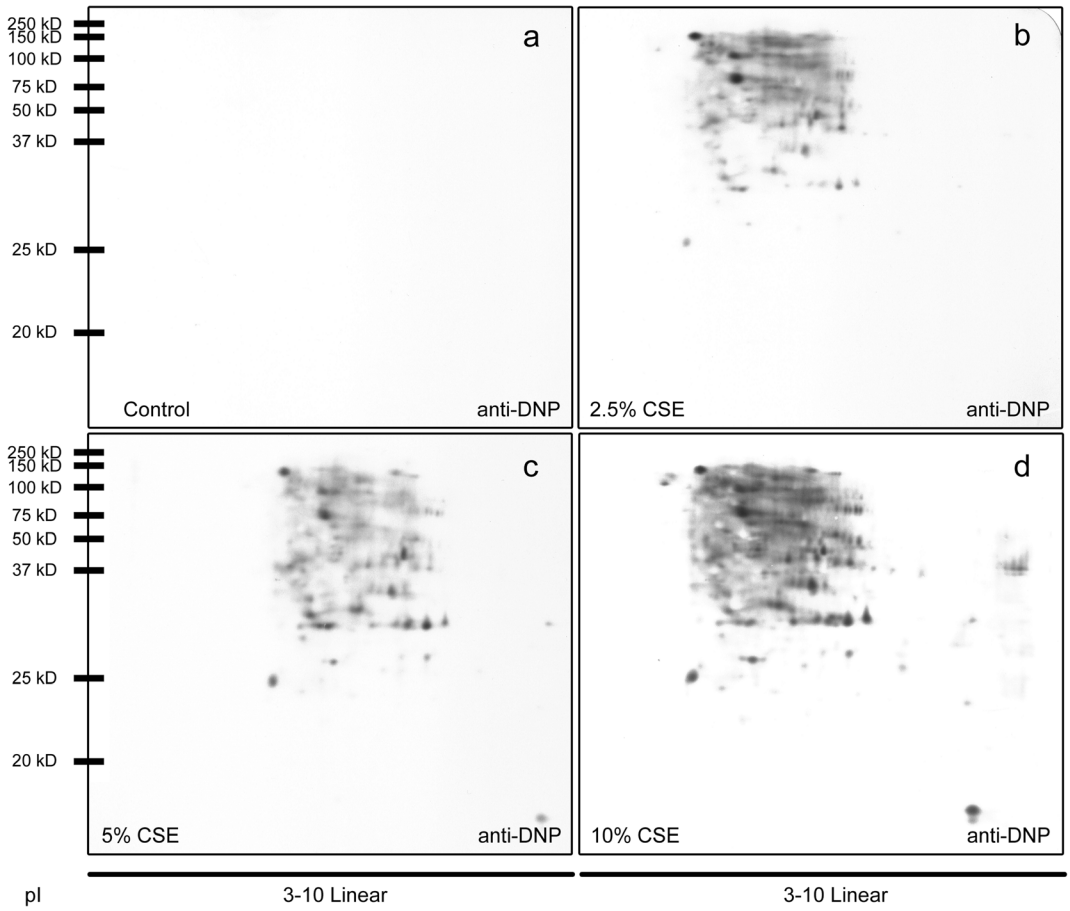

Fig. 4 Two-dimensional electrophoresis (2-D PAGE) separation and Western blot for assessing protein carbonylation. Representative 2-D Western blots of protein carbonylation in control 16-HBE cells (**a**) and 16-HBE cells exposed to 2.5% (**b**), 5% (**c**), and 10% (**d**) CSE are shown. After 2-D PAGE separation, proteins were blotted to PVDF membrane and derivatized with DNPH as described in "Materials and Methods"

metabolic processes such as energy generation, biosynthesis, nitrogen or phosphate-containing compound metabolism, catabolic and sulphur-containing compound metabolism is limited to 18%, 13%, 8%, 8%, 8%, and 4%, respectively (Fig. 6a). This functional classification suggests that protein and lipid metabolism are preferentially affected by CSE-induced protein carbonylation in 16-HBE cells. Furthermore, 57% of carbonylated proteins has catalytic activity; among which those with oxidoreductase, hydrolase, and isomerase activities are 42%, 17%, and 17 %, respectively (Fig. 6b).

Discussion and conclusion

In vivo, bronchial epithelial cells are located at the interface between airspace and the internal environment, so they are exposed to many pathogens and environmental stressors. Cigarette smoking is one of the most important environmental risk factor for the respiratory epithelium. CS induces oxidative damage due to two mechanisms: (i) it contains high levels of reactive species, so ROS and RNS (both radicals and non-radicals) are inhaled directly from a burning cigarette; (ii) CS can induce cellular production of oxidants by stimulating inflammatory cells (Kirkham and Rahman 2006). ROS and RNS are related to several airway pathologies such as cancer, COPD, and asthma (Colombo et al. 2014). CS induces damage to proteins and organelles by oxidative stress, resulting in accelerated respiratory epithelial cell senescence and affecting cell viability and proliferation. Although it is known that CS mediates oxidative damage in the cell (Colombo et al. 2014), limited information is available on the CS-induced oxidative damage of

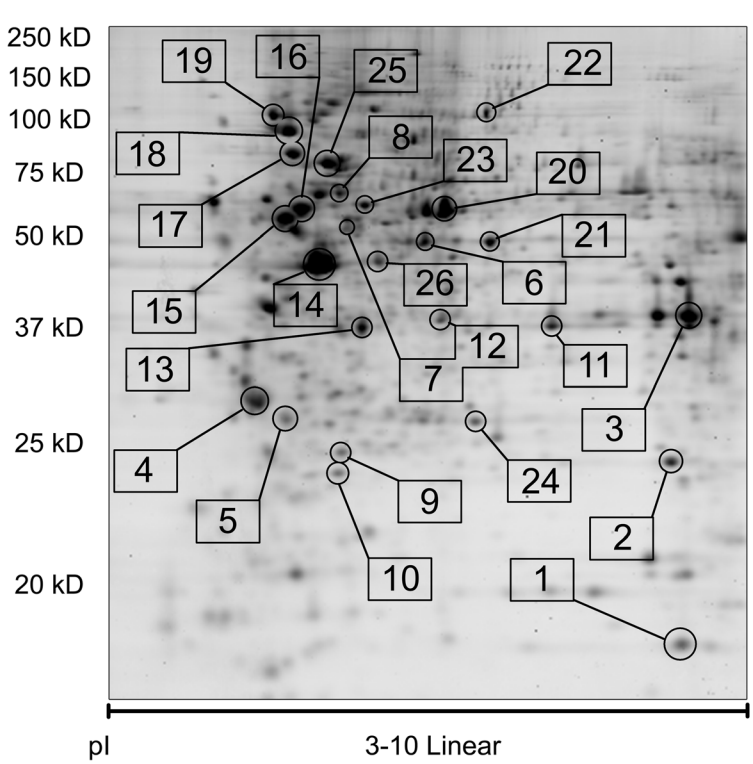

S1: Profilin-1
S2: Peroxiredoxin-1
S3: GAPDH
S4: 14-3-3 protein zeta/delta
S5: Rho GDP-dissociation I1
S6: Elongation factor 1-gamma
S7: RuvB-like 2
S8: T-complex protein 1 s theta
S9: Glutathione S-Transferase P
S10: Peroxiredoxin-2
S11: Annexin A2
S12: Annexin A1
S13: L-lactate DH B chain
S14: Actin cytoplasmic
S15: Tubulin beta chain
S16: Tubulin alpha-1c/1b chain
S17: 78kDa glucose regulated protein
S18: HSP 90-beta
S19: Endoplasmin
S20: Retinal dehydrogenase 1
S21: Alpha enolase
S22: Elongation factor 2
S23: Protein S-S isomerase A3
S24: Triosephosphate isomerase
S25: Heat shock cognate 71kDa protein
S26: Protein phosphate methylesterase

Fig. 5 Representative MS-compatible Silver stained 2-D gel of protein extracts from 16-HBE cells treated with 5% CSE for 3 hours with labelled locations of carbonylated proteins identified by MS. The 2-D gel image shows locations of 26 highly carbonylated proteins following 3-h exposure of 16-HBE cells to 5% CSE as detected by Western blot (Fig. 4c) and identified by means of MALDI-TOF MS approach and MASCOT database search. The identified carbonylated proteins are listed on the right and their details are reported in Table 1

proteins in human airway epithelial cells. Increased carbonylation of total proteins was seen in primary human bronchial epithelial cells obtained from smokers with COPD as well as in primary human bronchial epithelial cells and in A549 human alveolar epithelial cells exposed to CSE compared to their respective controls (Hara et al. 2012; van Rijt et al. 2012). Because bronchial epithelial cells represent the first line of defense against CS, we investigated the effect of exposure to CSE in 16-HBE cells, focussing on the oxi-proteome. CSE is useful to simulate exposure to CS and to study its effects in vitro (Colombo et al. 2012; Gornati et al. 2013; Kode et al. 2008) because it is easy to prepare, easy to use, and contains most of the chemicals inhaled by smokers (Dalle-Donne et al. 2016).

In this study, we observed that long time (> 24 h) exposure of 16-HBE cells to different concentrations of CSE markedly affected the cell growth in a dose-dependent way and resulted to be lethal at the highest concentration (Fig. 1a). A similar result was observed using MTT assay to assess cell metabolic activity (Fig. 1b). This colorimetric assay is based on the ability of viable cells to reduce a soluble yellow tetrazolium salt (MTT) to a blue formazan crystal by mitochondrial succinate dehydrogenase activity. Hence, the MTT assay is a good index of mitochondrial activity, being dependent on mitochondrial respiration, and thus of cell viability and indirectly serves to assess the energy capacity of a cell. A previous study suggests that the increased mortality of 16-HBE cells observed in the presence of 10% CSE for 24 h is not due to an apoptotic process (Bazzini et al. 2013), whereas another study showed that treatment of 16-HBE cells with 10% and 20% CSE for 24 h accelerates cell senescence (Tsuji et al. 2004).

Treatment with CSE dose-dependently decreased migration of 16-HBE cells (Fig. 2), which is in agreement with other studies showing reduction in human gingival epithelial cell growth after exposure to CSE (Colombo et al. 2012; Imamura et al. 2015). In addition, it was also shown that exposure to whole CS markedly inhibits human gingival epithelial cell growth and migration by both apoptosis and necrosis (Semlali et al. 2011).

Table 1 Identified carbonylated proteins in 16-HBE cells exposed to 5% CSE for 3 h

Spot no.	Identification	Mascot score	Sequence coverage (%)	Peptide match	MW (Da)	Calculated pI	SwissProt accession no.
S1	Profilin-1	61	39	6/17	15,216	8.44	P07737
S2	Peroxiredoxin-1	98	42	8/19	22,324	8.27	Q06830
S3	Glyceraldehyde-3-phosphate dehydrogenase	86	25	7/12	36,201	8.57	P04406
S4	14-3-3 protein zeta/delta	74	31	10/22	27,899	4.73	P63104
S5	Rho GDP-dissociation inhibitor 1	63	38	6/18	23,250	5.02	P52565
S6	Elongation factor 1-gamma	72	19	8/21	50,429	6.25	P26641
S7	RuvB-like 2	57	22	7/19	51,296	5.49	Q9Y230
S8	T-complex protein 1 subunit theta	58	16	7/25	60,153	5.42	P50990
S9	Glutathione S-transferase P	73	40	5/8	23,569	5.43	P09211
S10	Peroxiredoxin-2	58	18	4/6	22,049	5.66	P32119
S11	Annexin A2	135	35	11/14	38,808	7.57	P07355
S12	Annexin A1	78	23	7/11	38,918	6.57	P04083
S13	L-lactate dehydrogenase B chain	76	27	9/20	36,900	5.71	P07195
S14	Actin, cytoplasmic 1	100	29	8/13	42,052	5.29	P60709
	Actin, cytoplasmic 2	100	29	8/13	42,108	5.31	P63261
S15	Tubulin beta chain	124	24	12/17	50,095	4.78	P07437
	Tubulin beta-4B chain	124	24	12/17	50,255	4.79	P68371
	Tubulin beta-2A chain	108	22	11/17	50,274	4.78	Q13885
	Tubulin beta-2B chain	108	22	11/17	50,377	4.78	Q9BVA1
	Tubulin beta-4A chain	75	16	8/17	50,010	4.78	P04350
	Tubulin beta-3 chain	60	16	8/17	50,856	4.83	Q13509
S16	Tubulin alpha-1C chain	115	24	8/8	50,548	4.96	Q9BQE3
	Tubulin alpha-1B chain	115	24	8/8	50,804	4.94	P68363
	Tubulin alpha-1A chain	92	21	7/8	50,788	4.94	Q71U36
	Tubulin alpha-4A chain	74	18	6/8	50,634	4.95	P68366
	Tubulin alpha-8 chain	74	18	6/8	50,746	4.95	Q9NY65
	Tubulin alpha-3C/D chain	57	16	5/8	50,612	4.96	Q13748
S17	78 kDa glucose-regulated protein	137	26	13/16	72,402	5.07	P11021
S18	Heat-shock protein HSP 90-beta	94	17	11/15	83,554	4.97	P08238
S19	Endoplasmin	75	14	10/14	92,696	4.76	P14625
S20	Retinal dehydrogenase 1	98	24	11/20	55,454	6.30	P00352
S21	Alpha-enolase	107	28	10/16	47,481	7.01	P06733
S22	Elongation factor 2	86	14	10/13	96,246	6.41	P13639
S23	Protein disulfide-isomerase A3	107	25	13/22	57,146	5.98	P30101
S24	Triosephosphate isomerase	64	36	6/17	31,057	5.65	P60174
S25	Heat-shock cognate 71 kDa protein	85	21	9/14	71,082	5.37	P11142
S26	Protein phosphatase methylesterase 1	76	23	8/14	42,687	5.67	Q9Y570

Spot number refers to labelled protein spots shown in Fig. 5

Exposure of 16-HBE cells to CSE (up to 24 h) increased carbonylation, as detected by both immunofluorescence and immunoblotting (Fig. 3). Carbonylation is diffused within the nucleus and cytoplasm of cells and increases in parallel with CSE concentration. This suggests that CSE reactive molecules can diffuse within intracellular compartments, including the nucleus. Interestingly, a decrease in protein carbonylation was

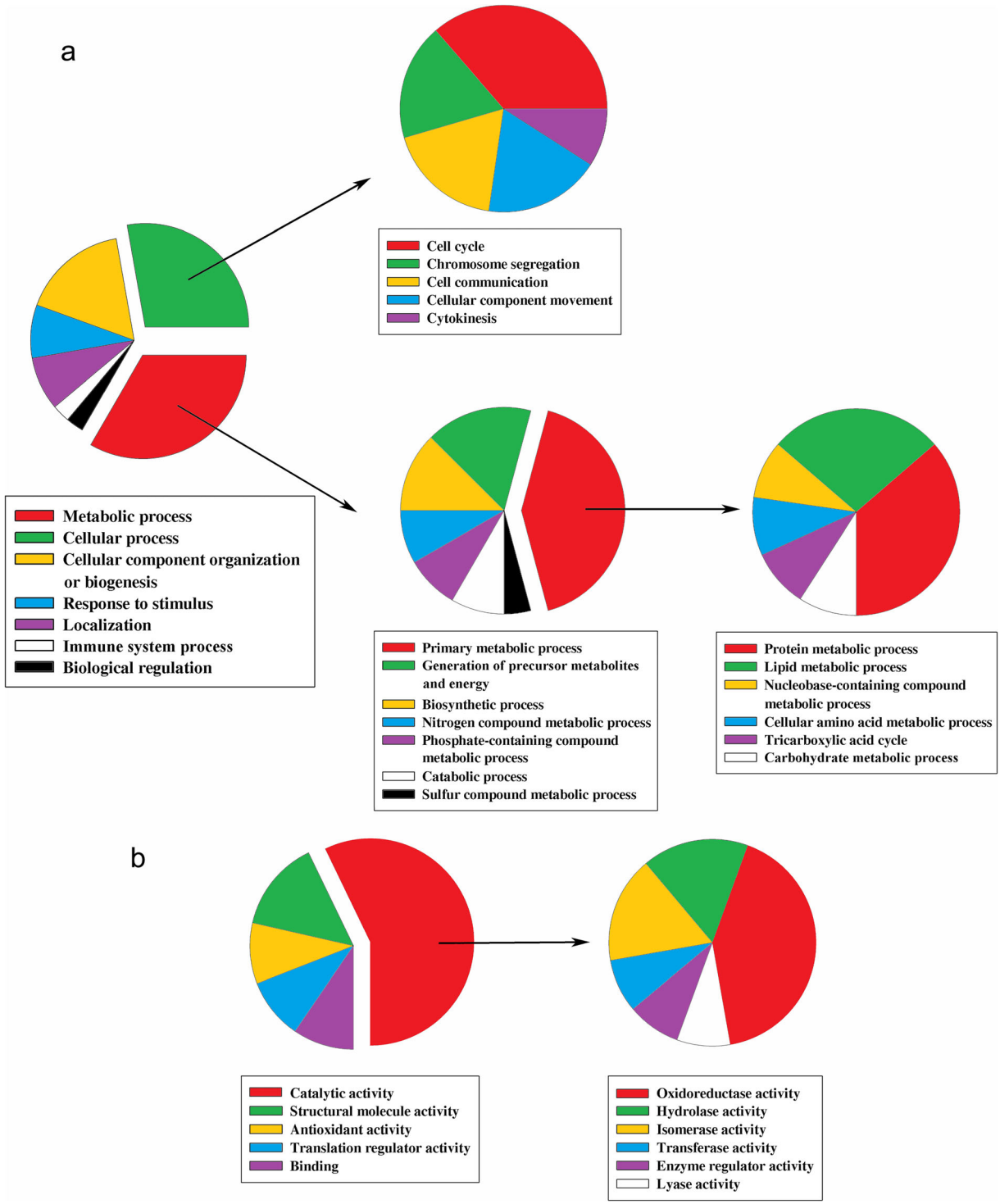

Fig. 6 Characterization of identified carbonylated proteins. Pie charts illustrating the classification of identified carbonylated proteins on the basis of (**a**) the biological processes in which they are mainly involved and (**b**) their main molecular functions, according to the PANTHER (Protein ANalysis THrough Evolutionary Relationships) Classification System (http://www.pantherdb.org/)

evident, both in immunofluorescence and in immunoblot experiments, after 24 h of cell exposure to CSE. This decrease in protein carbonylation may suggest the involvement of a protein recycling system capable of degrading carbonylated proteins and resynthesizing new proteins. We hypothesized that the ubiquitin–proteasome system was involved in the degradation of CSE-oxidized proteins (Erales and Coffino 2014), but the investigation of mono- and polyubiquitination by means of specific antibodies (mAb (FK2), Enzo Life Sciences) did not show any significant differences between control cells and cells exposed to 5–10–20% CSE for 3 and 24 h (data not shown). This observation suggests that carbonylated proteins could undergo degradation following an ubiquitin- and ATP-independent (20S-dependent) mechanism (Grune et al. 1997; Shringarpure et al. 2003). In fact, it is established that the 20S proteasome degrades most of all oxidized proteins in eukaryotic cells via the involvement of HSP70 (Jung et al. 2006; Höhn et al. 2014; Reeg et al. 2016) and the 11S proteasome facilitates this process under conditions of heightened oxidative stress (Jung et al. 2014). Moreover, it has been shown that carbonylated proteins are not preferentially ubiquitinated (Kästle and Grune 2011; Kästle et al. 2012).

By means of MALDI-TOF MS analysis, we identified many of the proteins undergoing carbonylation following cell exposure to CSE (Fig. 5 and Table 1). Among the identified proteins, there are many tubulin and actin isoforms (Table 1). Tubulin represents one of the most abundant proteins in a cell and, in 16-HBE cells exposed to CSE, it resulted to be one of the most carbonylated ones. Carbonylated tubulin and actin could be responsible for the observed reduction of cell migration and change in cell shape. A reduced cell viability, a round-shaped cell morphology, a disruption of the microtubule network, and oxidative damage of tubulin (visualized as protein carbonylation) were observed in human lung epithelial (A549) cells exposed to aqueous extract of CS (Das et al. 2009).

Actin filaments play central roles in the shaping, morphology, organization of cells, maintenance of cell integrity, and stability of cytoskeletal interactions, as well as cell substrate adhesion. Considering that cellular shrinkage and rounding depend on perturbation of filamentous actin, protein carbonylation is likely to be responsible, at least in part, for actin conformational changes and/or loss of function (Dalle-Donne et al. 2001; Castro et al. 2013), leading to change in actin and tubulin dynamics and resulting in altered cell shape, impaired cell migration, and reduced thickness of the growing cell layer, as observed after cell incubation with CSE (Fig. 2). Consistently, carbonylation of profilin-1 that we detected in 16-HBE cells exposed to CSE could induce alterations of the actin cytoskeleton contributing to the loss of its regulation (Shekhar et al. 2016).

Considering the numerous roles of microtubules and their dynamics in intracellular movements and cell motility, in the next future, we will investigate the effect of CSE-induced tubulin carbonylation on microtubule dynamics and we will try to identify, by means of a MS approach, the amino acid residues of tubulin undergoing carbonylation and the carbonylating agent(s).

Many of the carbonylated proteins identified in CSE-exposed 16-HBE cells are involved in energy metabolism. Carbonylation may impair protein function and, consequently, the energy production in 16-HBE cells. Among these carbonylated proteins, we identified glyceraldehyde-3-phosphate dehydrogenase (GAPDH), L-lactate dehydrogenase (LDH) B chain, and α-enolase. The latter, an enzyme that hydrolyses 2-phosphoglycerate to phosphoenol pyruvate in glycolysis, has recurrently emerged from redox proteomic studies as being very vulnerable to the products of lipid peroxidation (Reed et al. 2009; Sultana et al. 2013). This redox vulnerability has also been linked to a dose- and time-dependent reduction of plasminogen binding to α-enolase in HL-60 human leukaemic cells after HNE adducts formation (Gentile et al. 2009). In addition, α-enolase has also emerged as a common target of autoantibody formation in numerous autoimmune diseases, suggesting that peroxidative modifications might be instrumental in the breakage of immunological tolerance (Pizzimenti et al. 2013). The increased carbonylation of α-enolase and also GAPDH, which catalyses the oxidation of glyceraldehyde 3-phosphate to 1,3-bisphosphoglycerate and NADH, could lead to severely impaired glycolytic function and decreased ATP production, therefore decreasing the level of intracellular available energy, compromising basal and essential functions requiring the energy investment.

Carbonylation of some glycolytic enzymes and cytoskeletal proteins was also observed in primary human gingival fibroblasts (Colombo et al. 2012) and in the human umbilical vein endothelial cell line (ECV-304 cells) exposed to CSE (Gornati et al. 2013). In addition, several studies demonstrated that CS induces carbonylation of actin and other cytoskeletal proteins and enzymes involved in carbohydrate metabolism in both

smokers and animal models exposed to CS (Dalle-Donne et al. 2016). Therefore, we can assert that glycolytic enzymes and cytoskeletal proteins represent the primary targets of smoking.

As a whole, we can classify the 26 CSE-induced carbonylated proteins in a few functional groups (Fig. 6a, b) including primary metabolic processes, such as protein and lipid metabolism, fundamental cellular processes as cell cycle, chromosome aggregation and cytokinesis (the last two mainly depending on the microtubule and microfilament cytoskeleton, respectively), and regulating and communication processes. As a consequence of carbonylation, the structure and the function of these proteins can be altered leading to dysregulation of basic and crucial processes in cellular homeostasis. The redox proteomic literature clearly indicates that a primary role in the pathogenesis of oxidative stress-associated pathologies is played by the functional inactivation of crucial cell proteins, upon their covalent adduction by glycoxidation and/or lipid peroxidation products leading to protein carbonylation (Berlett and Stadtman 1997; Bachi et al. 2013). All studies agreed that vulnerable proteins could be mainly assigned to a few distinct functional groups with crucial roles in energy metabolism, cell signalling, cytoskeletal organization, antioxidant defenses, and cellular stress responses, in agreement with our conclusions. Moreover, cell proteome modifications induced by the products of glycoxidation and lipid peroxidation, in the course of oxidative stress or upon exposure to oxidizing compounds, emerge as a possibly unifying mechanism for many diseases which affect humans who adopt inappropriate lifestyles (such as smoking and excess food intake, not forgetting that AGEs and ALEs are both introduced with food and synthesized in our body as a consequence of excess caloric intake) (Ruskovska and Bernlohr 2013; Colombo et al. 2014; Dalle-Donne et al. 2016), or who are exposed to environmental pollutants (e.g., Niaz et al. 2017; Piao et al. 2018).

Acknowledgments This research was supported by the "Piano di Sostegno alla Ricerca 2016—Linea 2" (Università degli Studi di Milano).

Abbreviations *2D-GE*, 2Dgel electrophoresis; *Dinitrophenyl-KLH*, Keyhole limpet haemocyanin conjugate; *DNPH*, Dinitrophenyl hydrazine; *DTT*, Dithiothreitol; *ECL*, Enhanced chemiluminescence; *HMW*, High molecular weight; *HRP*, Horseradish peroxidase; *MALDI-TOF*, Matrix-assisted laser desorption/ionization time of flight; *MS*, Mass spectrometry

References

Adesina AM, Vallyathan V, McQuillen EN, Weaver SO, Craighead JE. Bronchiolar inflammation and fibrosis associated with smoking. Am Rev Respir Dis. 1991;143:144–9.

Afridi HI, Kazi TG, Talpur FN, Naher S, Brabazon D. Relationship between toxic metals exposure via cigarette smoking and rheumatoid arthritis. Clin Lab. 2014;60:1735–45.

Aiassa V, Baronetti JL, Paez PL, Barnes AI, Albrecht C, Pellarin G, et al. Increased advanced oxidation of protein products and enhanced total antioxidant capacity in plasma by action of toxins of Escherichia coli STEC. Toxicol in Vitro. 2011;25:426–31.

Alberg AJ, Brock MV, Ford JG, Samet JM, Spivack SD. Epidemiology of lung cancer: diagnosis and management of lung cancer, 3rd ed: American college of chest physicians evidence-based clinical practice guidelines. Chest. 2013;143:e1S–e29S.

Armstrong AW, Harskamp CT, Dhillon JS, Armstrong EJ. Psoriasis and smoking: a systematic review and meta-analysis. Br J Dermatol. 2014;170:304–14.

Bachi A, Dalle-Donne I, Scaloni A. Redox proteomics: chemical principles, methodological approaches and biological/biomedical promises. Chem Rev. 2013;113:596–698.

Bazzini C, Rossetti V, Civello DA, Sassone F, Vezzoli V, Persani L, et al. Short- and long- term effects of cigarette smoke exposure on glutathione homeostasis in human bronchial epithelial cells. Cell Physiol Biochem. 2013;32:129–45.

Bersaas A, Arnoldussen YJ, Sjøberg M, Haugen A, Mollerup S. Epithelial-mesenchymal transition and FOXA genes during tobacco smoke carcinogen induced transformation of human bronchial epithelial cells. Toxicol in Vitro. 2016;35:55–65.

Berlett S, Stadtman ER. Protein oxidation in aging, disease and oxidative stress. J Biol Chem. 1997;272:20313–6.

Bodas M, Van Westphal C, Carpenter-Thompson R, Mohanty D, Vij N. Nicotine exposure induces bronchial epithelial cell apoptosis and senescence via ROS mediated autophagy-impairment. Free Radic Biol Med. 2016;97:441–53.

Bondì ML, Ferraro M, Di Vincenzo S, Gerbino S, Cavallaro G, Giammona G, et al. Effects in cigarette smoke stimulated bronchial epithelial cells of a corticosteroid entrapped into nanostructured lipid carriers. J Nanobiotechnology. 2014;29:12–46.

Bose T. Bitter correlationship between autoimmune hepatitis and smoking. Med Hypotheses. 2015;84:118–21.

Brusselle GG, Joos GF, Bracke KR. New insights into the immunology of chronic obstructive pulmonary disease. Lancet. 2011;378:1015–26.

Bucchieri F, Marino Gammazza A, Pitruzzella A, Fucarino A, Farina F, Howarth P, et al. Cigarette smoke causes caspase-independent apoptosis of bronchial epithelial cells from asthmatic donors. PLoS One. 2015;10:1–15.

Castro JP, Ott C, Jung T, Grune T, Almeida H. Carbonylation of the cytoskeletal protein actin leads to aggregate formation. Free Radic Biol Med. 2012;53:916–25.

Castro JP, Jung T, Grune T, Almeida H. Actin carbonylation: from cell dysfunction to organism disorder. J Proteome. 2013;92:171–80.

Chang D, Sha Q, Zhang X, Liu P, Rong S, Han T, et al. The evaluation of the oxidative stress parameters in patients with primary angle-closure glaucoma. PLoS One. 2011;6:4–9.

Colombo G, Rusconi F, Rubino T, Cattaneo A, Martegani E, Parolaro D, et al. Transcriptomic and proteomic analyses of mouse cerebellum reveals alterations in RasGRF1 expression following in vivo chronic treatment with delta 9-tetrahydrocannabinol. J Mol Neurosci. 2009;37:111–22.

Colombo G, Dalle-Donne I, Orioli M, Giustarini D, Rossi R, Clerici M, et al. Oxidative damage in human gingival fibroblasts exposed to cigarette smoke. Free Radic Biol Med. 2012;52:1584–96.

Colombo G, Clerici M, Giustarini D, Portinaro NM, Aldini G, Rossi R, et al. Pathophysiology of tobacco smoke exposure: recent insights from comparative and redox proteomics. Mass Spectrom Rev. 2014;33:183–218.

Colombo G, Clerici M, Garavaglia ME, Giustarini D, Rossi R, Milzani A, et al. A step-by-step protocol for assaying protein carbonylation in biological samples. J Chromatogr B Anal Technol Biomed Life Sci. 2016;1019:178–90.

Costenbader KH, Karlson EW. Cigarette smoking and autoimmune disease: what can we learn from epidemiology? Lupus. 2006;15:737–45.

Das A, Bhattacharya A, Chakrabarti G. Cigarette smoke extract induces disruption of structure and function of tubulin-microtubule in lung epithelium cells and in vitro. Chem Res Toxicol. 2009;22:446–59.

Dalle-Donne I, Rossi R, Giustarini D, Gagliano N, Lusini L, Milzani A, et al. Actin carbonylation: from a simple marker of protein oxidation to relevant signs of severe functional impairment. Free Radic Biol Med. 2001;31:1075–83.

Dalle-Donne I, Rossi R, Giustarini D, Milzani A, Colombo R. Protein carbonyl groups as biomarkers of oxidative stress. Clin Chim Acta. 2003;329:23–38.

Dalle-Donne I, Aldini G, Carini M, Colombo R, Rossi R, Milzani A. Protein carbonylation, cellular dysfunction, and disease progression. J Cell Mol Med. 2006;10:389–406.

Dalle-Donne I, Colombo G, Gornati R, Garavaglia ML, Portinaro N, Giustarini D, et al. Protein carbonylation in human smokers and mammalian models of exposure to cigarette smoke: focus on redox proteomic studies. Antioxid Redox Signal. 2016;26:406–26.

Dietrich T, Bernimoulin JP, Glynn RJ. The effect of cigarette smoking on gingival bleeding. J Periodontol. 2004;75:16–22.

Dong R, Xie L, Zhao K, Zhang Q, Zhou M, He P. Cigarette smoke-induced lung inflammation in COPD mediated via LTB4/BLT1/SOCS1 pathway. Int J Chron Obstruct Pulmon Dis. 2015;11:31–41.

Erales J, Coffino P. Ubiquitin-independent proteasomal degradation. Biochim Biophys Acta, Mol Cell Res. 2014;1843:216–21.

Feng J, Xie H, Meany DL, Thompson LV, Arriaga EA, Griffin TJ. Quantitative proteomic profiling of muscle type-dependent and age-dependent protein carbonylation in rat skeletal muscle mitochondria. J Gerontol A Biol Sci Med Sci. 2008;63:1137–52.

Gentile F, Pizzimenti S, Arcaro A, Pettazzoni P, Minelli R, D'Angelo D, et al. Exposure of HL-60 human leukaemic cells to 4-hydroxynonenal promotes the formation of adduct(s) with alpha-enolase devoid of plasminogen binding activity. Biochem J. 2009;422:285–94.

Gornati R, Colombo G, Clerici M, Rossi F, Gagliano N, Riva C, et al. Protein carbonylation in human endothelial cells exposed to cigarette smoke extract. Toxicol Lett. 2013;218:118–28.

Grune T, Reinheckel T, Davies KJ. Degradation of oxidized proteins in mammalian cells. FASEB J. 1997;11:526–34.

Hara H, Araya J, Takasaka N, Fujii S, Kojima J, Yumino Y, et al. Involvement of creatine kinase B in cigarette smoke-induced bronchial epithelial cell senescence. Am J Respir Cell Mol Biol. 2012;46:306–12.

Hogg JC, McDonough JE, Suzuki M. Small airway obstruction in COPD: new insights based on micro-CT imaging and MRI imaging. Chest. 2013;143:1436–43.

Höhn A, Jung T, Grune T. Pathophysiological importance of aggregated damaged proteins. Free Radic Biol Med. 2014;71:70–89.

Huang MF, Lin WL, Ma YC. A study of reactive oxygen species in mainstream of cigarette. Indoor Air. 2005;15:135–40.

Imamura K, Kokubu E, Kita D, Ota K, Ishihara K, Saito A. Cigarette smoke condensate modulates migration of human gingival epithelial cells and their interactions with Porphyromonas gingivalis. J Periodontal Res. 2015;50:411–21.

Jang J, Bruse S, Liu Y, Duffy V, Zhang C, Oyamada N, et al. Aldehyde dehydrogenase 3A1 protects airway epithelial cells from cigarette smoke-induced DNA damage and cytotoxicity. Free Radic Biol Med. 2014;68:80–6.

Jung T, Engels M, Kaiser B, Poppek D, Grune T. Intracellular distribution of oxidized proteins and proteasome in HT22 cells during oxidative stress. Free Radic Biol Med. 2006;40:1303–12.

Jung T, Höhn A, Grune T. The proteasome and the degradation of oxidized proteins: part II—protein oxidation and proteasomal degradation. Redox Biol. 2014;2:99–104.

Kästle M, Grune T. Proteins bearing oxidation-induced carbonyl groups are not preferentially ubiquitinated. Biochimie. 2011;96:1076–9.

Kästle M, Reeg S, Rogowska-Wrzesinska A, Grune T. Chaperones, but not oxidized proteins, are ubiquitinated after oxidative stress. Free Radic Biol Med. 2012;53:1468–77.

Kirkham P, Rahman I. Oxidative stress in asthma and COPD: antioxidants as a therapeutic strategy. Pharmacol Ther. 2006;111:476–94.

Kode A, Rajendrasozhan S, Caito S, Yang SR, Megson IL, Rahman I. Resveratrol induces glutathione synthesis by activation of Nrf2 and protects against cigarette smoke-mediated oxidative stress in human lung epithelial cells. Am J Phys Lung Cell Mol Phys. 2008;294:L478–88.

Liu A, Wu J, Li A, Bi W, Liu T, Cao L, et al. The inhibitory mechanism of Cordyceps sinensis on cigarette smoke extract-induced senescence in human bronchial epithelial cells. Int J Chron Obstruct Pulmon Dis. 2016;11:1721–31.

Niaz K, Mabqool F, Khan F, Ismail Hassan F, Baeeri M, Navaei-Nigjeh M, et al. Molecular mechanisms of action of styrene toxicity in blood plasma and liver. Environ Toxicol. 2017;32(10):2256–66. https://doi.org/10.1002/tox.22441.

Mak A, Tay SH. Environmental factors, toxicants and systemic lupus erythematosus. Int J Mol Sci. 2014;15:16043–56.

Martínez A, Portero-Otin M, Pamplona R, Ferrer I. Protein targets of oxidative damage in human neurodegenerative diseases

with abnormal protein aggregates. Brain Pathol. 2010;20: 281–97.

McDonough JE, Yuan R, Suzuki M, Seyednejad N, Elliot WM, Sanchez PG, et al. Small airway obstruction and emphysema in chronic obstructive pulmonary disease. N Engl J Med. 2011;365:1567–75.

Morris PB, Ference BA, Jahangir E, Feldman DN, Ryan JJ, Bahrami H, et al. Cardiovascular effects of exposure to cigarette smoke and electronic cigarettes: clinical perspectives from the Prevention of Cardiovascular Disease Section Leadership Council and Early Career Councils of the American College of Cardiology. J Am Coll Cardiol. 2015;66:1378–91.

Morse D, Rosas IO. Tobacco smoke-induced lung fibrosis and emphysema. Annu Rev Physiol. 2014;76:493–513.

Mortaz E, Folkerts G, Redegeld F. Mast cells and COPD. Pulm Pharmacol Ther. 2011;24:367–72.

Pace E, Ferraro M, Di Vincenzo S, Cipollina C, Gerbino S, Cigna D, et al. Comparative cytoprotective effects of carbocysteine and fluticasone propionate in cigarette smoke extract-stimulated bronchial epithelial cells. Cell Stress Chaperones. 2013;18:733–43.

Perricone C, Versini M, Ben-Ami D, Gertel S, Watad A, Segel MJ, et al. Smoke and autoimmunity: the fire behind the disease. Autoimmun Rev. 2016;15:354–74.

Piao MJ, Ahn MJ, Kang KA, Ryu YS, Hyun YJ, Shilnikova K, et al. Particulate matter 2.5 damages skin cells by inducing oxidative stress, subcellular organelle dysfunction, and apoptosis. Arch Toxicol. 2018;92(6):2077–91. https://doi.org/10.1007/s00204-018-2197-9.

Pizzimenti S, Ciamporcero E, Daga M, Pettazzoni P, Arcaro A, Cetrangolo G, et al. Interaction of aldehydes derived from lipid peroxidation and membrane proteins. Front Physiol. 2013;4:242.

Rahman I. Oxidative stress in pathogenesis of chronic obstructive pulmonary disease: cellular and molecular mechanisms. Cell Biochem Biophys. 2005;43:167–88.

Reed TT, Pierce WM, Markesbery WR, Butterfield DA. Proteomic identification of HNE-bound proteins in early Alzheimer disease: insights into the role of lipid peroxidation in the progression of AD. Brain Res. 2009;1274:66–76.

Reeg S, Jung T, Castro JP, Davies KJA, Henze A, Grune T. The molecular chaperone Hsp70 promotes the proteolytic removal of oxidatively damaged proteins by the proteasome. Free Radic Biol Med. 2016;99:153–66.

Ruskovska T, Bernlohr DA. Oxidative stress and protein carbonylation in adipose tissue - implications for insulin resistance and diabetes mellitus. J Proteome. 2013;92:323–34.

Saetta M, Turato G, Baraldo S, Zanin A, Braccioni F, Mapp CE, et al. Goblet cell hyperplasia and epithelial inflammation in peripheral airways of smokers with both symptoms of chronic bronchitis and chronic airflow limitation. Am J Respir Crit Care Med. 2000;161:1016–21.

Semlali A, Chakir J, Goulet JP, Chmielewski W, Rouabhia M. Whole cigarette smoke promotes human gingival epithelial cell apoptosis and inhibits cell repair processes. J Periodontal Res. 2011;46:533–41.

Sethi S, Muscarella K, Evans N, Klingman KL, Grant BJB, Murphy TF. Airway inflammation and etiology of acute exacerbations of chronic bronchitis. Chest. 2000;118:1557–65.

Shekhar S, Pernier J, Carlier MF. Regulators of actin filament barbed ends at a glance. J Cell Sci. 2016;129:1085–91.

Shringarpure R, Grune T, Mehlhase J, Davies KJ. Ubiquitin conjugation is not required for the degradation of oxidized proteins by proteasome. J Biol Chem. 2003;278:311–8.

Su Y, Cao W, Han Z, Block ER. Cigarette smoke extract inhibits angiogenesis of pulmonary artery endothelial cells: the role of calpain. Am J Phys Lung Cell Mol Phys. 2004;287:L794–800.

Sultana R, Perluigi M, Butterfield DA. Lipid peroxidation triggers neurodegeneration: a redox proteomics view into the Alzheimer disease brain. Free Radic Biol Med. 2013;62: 157–69.

Talbot J, Peres RS, Pinto LG, Oliveira RDR, Lima KA, Donate PB, et al. Smoking-induced aggravation of experimental arthritis is dependent of aryl hydrocarbon receptor activation in Th17 cells. Arthritis Res Ther. 2018;20:119.

Tesfaigzi Y. Roles of apoptosis in airway epithelia. Am J Respir Cell Mol Biol. 2006;34:537–47.

Thorley AJ, Tetley TD. Pulmonary epithelium, cigarette smoke, and chronic obstructive pulmonary disease. Int J Chron Obstruct Pulmon Dis. 2007;2:409–28.

Tsuji T, Aoshiba K, Nagai A. Cigarette smoke induces senescence in alveolar epithelial cells. Am J Respir Cell Mol Biol. 2004;31:643–9.

van Rijt SH, Keller IE, John G, Kohse K, Yildirim AÖ, Eickelberg O, et al. Acute cigarette smoke exposure impairs proteasome function in the lung. Am J Phys Lung Cell Mol Phys. 2012;303:L814–23.

Wong J, Magun B, Wood L. Lung inflammation caused by inhaled toxicants: a review. Int J Chron Obstruct Pulmon Dis. 2016;11:1391–401.

Wu D, Yuan Y, Lin Z, Lai T, Chen M, Li W, et al. Cigarette smoke extract induces placental growth factor release from human bronchial epithelial cells via ROS/MAPK (ERK-1/2)/Egr-1 axis. Int J Chron Obstruct Pulmon Dis. 2016;11:3031–42.

Xueshibojie L, Duo Y, Tiejun W. Taraxasterol inhibits cigarette smoke-induced lung inflammation by inhibiting reactive oxygen species-induced TLR4 trafficking to lipid rafts. Eur J Pharmacol. 2016;789:301–7.

Yadav P, Ellinghaus D, Rémy G, Freitag-Wolf S, Cesaro A, Degenhardt F, et al. Genetic factors interact with tobacco smoke to modify risk for inflammatory bowel disease in humans and mice. Gastroenterology. 2017;153:550–65.